Putidaredoxin-to-Cytochrome P450cam Electron Transfer: Differences between the Two Reductive Steps Required for Catalysis†

Vadim Yu. Kuznetsov,‡,§ Thomas L. Poulos,‡,||,⊥,# and Irina F. Sevrioukova*,‡

Departments of Molecular Biology and Biochemistry, Physiology and Biophysics, and Chemistry and Center in Chemical and Structural Biology, University of California, Irvine, California 92697-3900

Received June 5, 2006; Revised Manuscript Received July 10, 2006

ABSTRACT: Cytochrome P450cam (P450cam) is the terminal monooxygenase in a three-component camphor-hydroxylating system from *Pseudomonas putida*. The reaction cycle requires two distinct electron transfer (ET) processes from the [2Fe-2S] containing putidaredoxin (Pdx) to P450cam. Even though the mechanism of interaction and ET between the two proteins has been under investigation for over 30 years, the second reductive step and the effector role of Pdx are not fully understood. We utilized mutagenesis, kinetic, and computer modeling approaches to better understand differences between the two Pdx-to-P450cam ET events. Our results indicate that interacting residues and the ET pathways in the complexes formed between reduced Pdx (Pdx^r) and the ferric and ferrous dioxygen-bound forms of P450cam (oxy-P450cam) are different. Pdx Asp38 and Trp106 were found to be key players in both reductive steps. Compared to the wild-type Pdx, the D38A, W106A, and Δ106 mutants exhibited considerably higher K_d values for ferric P450cam and retained ca. 20% of the first electron transferring ability. In contrast, the binding affinity of the mutants for oxy-P450cam was not substantially altered while the second ET rates were <1%. On the basis of the kinetic and modeling data we conclude that (i) P450cam−Pdx interaction is highly specific in part because it is guided/controlled by the redox state of *both* partners; (ii) there are alternative ET routes from Pdx^r to ferric P450cam and a unique pathway to oxy-P450cam involving Asp38; (iii) Pdx Trp106 is a key structural element that couples the second ET event to product formation possibly via its "push" effect on the heme-binding loop.

Cytochromes P450 (P450) participate in a variety of metabolic processes and catalyze the monooxygenation of a wide range of aromatic and aliphatic substrates. Mixed function oxidation reactions catalyzed by P450s (Figure 1) require an input of two electrons that originate from NAD(P)H and are supplied by redox-linked proteins. The most extensively characterized P450, a camphor-hydroxylating cytochrome P450cam (P450cam)[1] from *Pseudomonas putida*, receives reducing equivalents from a [2Fe-2S] ferredoxin, putidaredoxin (Pdx), which shuttles between the hemoprotein and a FAD-containing putidaredoxin reductase (Pdr) (*1*). Protein−protein interactions in P450cam monooxygenase are highly specific, and neither Pdx nor Pdr is functionally interchangeable with the homologous proteins from other redox systems (*2*−*4*). The strict requirement of Pdx for reduction of ferrous dioxygen-bound P450cam (oxy-P450cam) and product formation is thought to be due to its unique ability to couple electron flow to successful substrate turnover (*3*, *5*, *6*). Owing to technical difficulties in monitoring oxy-P450cam reduction, this process remains the least studied in the P450cam catalytic cycle. However, earlier work has shown that the two ET reactions between reduced Pdx (Pdx^r) and ferric and oxy-P450cam may differ in the affinity, binding sites, or reaction mechanism (*7*−*10*).

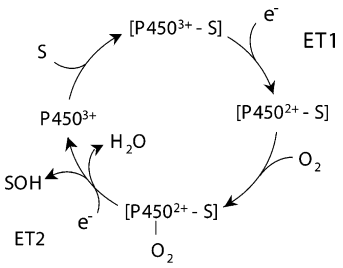

FIGURE 1: Fundamental cycle of cytochrome P450: $P450^{3+}$, resting state; S, substrate; [$P450^{3+}$-S], substrate-bound ferric form; [$P450^{2+}$-S], substrate-bound ferrous form; [O_2-$P450^{2+}$-S], dioxygen- and substrate-bound ferrous form; SOH, hydroxylated substrate. In P450cam monooxygenase, the first electron (ET1) can be transferred to P450cam from any reducing agent with a suitable redox potential, but only Pdx can deliver the second electron (ET2).

The underlying mechanism for the coupling effector role of Pdx is also unclear. Utilization of spectroscopic, kinetic,

† This research was supported by National Institutes of Health Grants GM67637 (to I.F.S.) and GM33688 (to T.L.P.).

* To whom correspondence should be addressed. Tel: 949-824-1953. Fax: 949-824-3280. E-mail: sevrioui@uci.edu.

‡ Department of Molecular Biology and Biochemistry, University of California.

§ Present address: Russian Research Institute of Physical Culture and Sport, Moscow 107005, Russia.

|| Department of Physiology and Biophysics, University of California.

⊥ Department of Chemistry, University of California.

Center in Chemical and Structural Biology, University of California.

[1] Abbreviations: P450cam, cytochrome P450cam from *Pseudomonas putida*; oxy-P450cam, the ferrous, dioxygen-bound form of P450cam; Pdx^o and Pdx^r, oxidized and reduced forms of putidaredoxin, respectively; Pdr, putidaredoxin reductase; ET, electron transfer; ET1 and ET2, the first and the second electron transfer to P450cam; WT, wild type; CoQ_0, 1,3-dimethoxy-5-methyl-1,4-benzoquinone.

10.1021/bi0611154 CCC: $33.50
Published on Web 09/07/2006

mutagenesis, NMR, and crystallographic techniques, as well as computer modeling and theoretical calculations (reviewed in refs *11* and *12*) has helped to establish that the Pdx binding/electron transfer (ET) site is located on the proximal surface of P450cam, the nearest approach to the buried heme cofactor and its cysteine ligand, Cys357 (*10*, *13*−*15*). Currently, two mechanisms for the specific effector action of Pdx have been proposed. According to the first, docking of Pdx to the proximal side of P450cam causes a "push" effect on the heme-binding loop and enhances electron donation from the axial thiolate to the heme iron, which in turn facilitates ET to the oxygenated hemoprotein and assists in scission of the O−O bond. This mechanism is based on theoretical and experimental data demonstrating the importance of thiolate ligation (reviewed in ref (*16*) and the Fe−S bond perturbation upon P450cam−Pdx complex formation (*17*−*20*). In an extended version of the proximal push mechanism, the binding of Pdx results in changes in the distal O_2 and substrate-binding pockets that lower the activation energy barrier required for electron transfer and O_2 activation (*21*, *22*). In the second mechanism, Pdx acts as an effector by restricting available conformations of P450cam to those that prevent the substrate/intermediate loss. This model is supported by NMR data indicating that Pdx^r binding causes perturbations in areas remote from the proximal face of P450cam, in particular, in the regions implicated in substrate access and orientation in the distal pocket (*23*, *24*).

On the basis of the X-ray and NMR structures of P450cam and Pdx, respectively, Pochapsky and co-workers (*15*) generated a model of the P450cam−Pdx complex that has served as a valuable structural guide for investigating redox partner interactions. However, the 1PUT Pdx structure (*25*) used by the Pochapsky group for model building differs significantly from the high-resolution X-ray structures (*26*, *27*) and a refined solution model of the iron−sulfur protein (*28*). Another limitation on the P450cam−Pdx model is that both protein structures are in the oxidized state. Redox-dependent conformational changes in Pdx, detected by NMR and X-ray crystallography methods (*28*−*32*), are significant and involve not only residues surrounding the metal cluster but also structural elements located in remote areas, including the Ile32−Asp38 peptide and Arg66. The redox-linked structural differences must be taken into account while modeling P450cam−Pdx interactions because the physiologically relevant redox partner of P450cam is Pdx^r.

In our previous study on the Pdx−Pdr interaction, we investigated the functional role of two residues that undergo major conformational perturbation upon Pdx reduction, Tyr33 and Arg66 (*32*), as well as Asp38 and Trp106 (Figure 2) (*33*). Changes in ET kinetics caused by various mutations were found to be in good agreement with theoretical predictions suggesting that Tyr33, Arg66, and Trp106 regulate Pdx−Pdr association by controlling how close Pdx can approach Pdr and that reduction driven movements of Tyr33 and Arg66 could facilitate Pdx dissociation upon ET completion. Insights gained from our work on the Pdx−Pdr system and the availability of crystal structures for reduced and oxidized Pdx as well as oxy-P450cam (*26*, *34*, *35*) prompted us to re-examine the Pdx−P450cam system. In this study we have used mutagenesis, kinetic, and computer modeling methods to test the role of specific residues in the reduction of both ferric and oxy-P450cam. Taken together, our experimental and modeling results provide an explanation for why the P450cam−Pdx interaction is highly specific and how Pdx may execute its effector role.

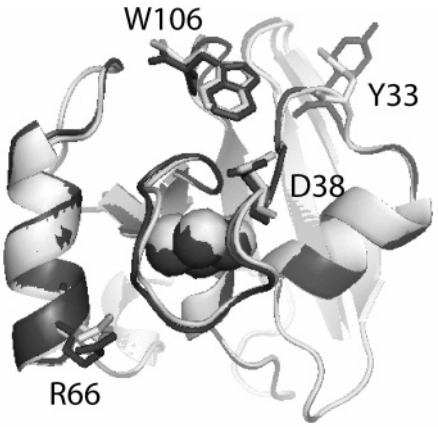

FIGURE 2: A view at the active site of Pdx. The least-squares superposition of the crystal structures of oxidized (white) and reduced (black) C73S Pdx molecules [molecules B, PDB codes 1XLP and 1XLQ, respectively (*32*)] was performed using the program LSQMAN (*78*). The [2Fe-2S] metal center and the mutated residues are shown in CPK and ball-and-stick representation, respectively.

EXPERIMENTAL PROCEDURES

Protein Expression and Purification. Pdx, P450cam, and Pdr were expressed and purified as described previously (*26*, *33*, *36*, *37*).

Spectroscopic and Stopped-Flow Assays. All conventional UV−visible spectroscopy was performed using a Cary 3 spectrophotometer. Stopped-flow experiments were carried out on an SX.18MV instrument (Applied Photophysics). Solutions were made anaerobic by multiple evacuation and flushing with prepurified argon and included an oxygen-scrubbing system consisting of 1 mM glucose and 1 unit/mL glucose oxidase and catalase. Reduction and oxidation of 40−50 μM Pdx with 5 mM sodium dithionite and 100 μM 1,3-dimethoxy-5-methyl-1,4-benzoquinone (CoQ_0), respectively, were carried out in 100 mM phosphate buffer, pH 7.5, and monitored at 456 nm at 5−35 °C. Prior to reacting with CoQ_0, Pdx was reduced using catalytic amounts of Pdr and subequimolar concentrations of NADH. In case of the D38A mutant, which was found to form a complex with CoQ_0, the oxidant concentration was 50 μM. The CoQ_0 reductase activity of this mutant was compared to that of WT measured under identical conditions. The kinetic data were analyzed using IgorPro software (WaveMetrics, Inc.). Activation energies (E_a) and logarithms of preexponential frequency factors (ln A) for the reactions of Pdx reduction and oxidation were calculated from the plots of ln k vs $1/T$ according to the Arrhenius equation

$$\ln k = \ln A - E_a/RT \quad (1)$$

Free energies ($\Delta G°$) were determined from the equation

$$\Delta G° = -nF\Delta E_m$$

where n is a number of electrons transferred during the reaction, F is the Faraday constant, and ΔE_m is a difference

between the redox potentials of an electron donor and acceptor. The $E_{1/2}$ values for sodium dithionite, CoQ_0, and WT Pdx used in calculations were −679 (*38*), +100, and −240 mV (*39*), respectively. The redox potentials of Pdx mutants measured by cyclic voltammetry (*33*) were adjusted by −78 mV to correct methodical differences. Apparent reorganization energies (λ) were calculated from the Marcus equation

$$E_a = (\lambda + \Delta G^\circ)^2/4\lambda \quad (2)$$

Measurement of the First and the Second Electron Transfer to P450cam. Transfer of the first electron from reduced Pdx to P450cam was measured in carbon monoxide saturated 50 mM phosphate buffer, pH 7.5, containing 100 mM KCl, 1 mM camphor, and an oxygen-scrubbing system, using a stopped-flow spectrophotometer. Solutions of 2 μM P450cam were mixed with various concentrations of Pdx^r. Formation of the ferrous−CO form of P450cam was monitored at 446 nm at 25 °C. The ET rates to the dioxygen adduct of ferrous P450cam (oxy-P450cam) were determined at 4 °C by following degradation of oxy-P450cam into ferric enzyme and hydroxycamphor at 390 nm according to the previously described procedure (*40*) using the sequential double mixing mode of the stopped-flow spectrophotometer. Solutions of 5 μM P450cam reduced with subequimolar amounts of sodium dithionite were first mixed with air-saturated buffer and, after a 1 s delay, with 4−50 μM Pdx^r. The k_{cat} and K_d values for the first and second ET reactions were determined from the hyperbolic plots of k_{obs} vs [Pdx].

Computer Modeling Studies. The program GRAMM that uses a surface complementarity algorithm for protein docking (*41*) was utilized to find possible conformations for the P450cam−Pdx ET complex. The program places each molecule on a grid and performs an exhaustive six-dimensional search through the relative intermolecular translations and rotations using a very efficient fast Fourier transform correlation technique and a simple scoring function that measures shape complementarity and penalizes overlaps. Crystal structures of oxidized (Pdx^o) and reduced Pdx [molecules B of 1XLP and 1XLQ, respectively (*32*)] and those of ferric [molecule A of 1DZ4 (*42*)] and ferrous, dioxygen-bound P450cam [molecule A (*35*)] without hydrogen atoms were used as input to GRAMM that was run in generic matching and hydrophobic docking modes with a 2.1 Å grid step for translations and 10° increments for rotations. Computer-generated complexes were analyzed to define preferred Pdx docking regions on the surface of P450cam and to select models where the heme−[2Fe-2S] distance was within the physiological ET range (<20 Å). The plausible models were optimized by adjusting side chain positions of interacting amino acid residues using the program "O" (*43*), and the resulting structures were energy minimized in CNS (*44*) using CHARMM-based force field and parameter and topology files provided with the package.

Other Calculations. Possible ET pathways between the redox centers in the model P450cam−Pdx complexes were predicted and analyzed using the program HARLEM (*45*) with default settings. Either single iron atoms or the entire cofactors were defined as electron donor/acceptor groups. The interface surface area in the P450cam−Pdx complexes was calculated using GRASP (*46*). Figures were prepared with MOLSCRIPT (*47*), RASTER3D (*48*), and PyMOL (*49*).

RESULTS AND DISCUSSION

Effect of Mutations on the Electron-Accepting and -Donating Ability of Pdx. Key Pdx residues that are either known or predicted to be important in redox partner recognition and ET include Tyr33, Asp38, Arg66, and Trp106 (Figure 2). Cyclic voltammetry measurements carried out in our previous study revealed significant variations in the kinetic reversibility of the oxidation/reduction process in WT and mutants of Pdx, suggesting that structural reorganization in the protein is coupled to the ET event (*33*). To better understand the mechanism of redox-dependent perturbations, we estimated activation (E_a) and reorganization (λ) energies for Pdx reduction and oxidation using sodium dithionite and CoQ_0 as a reductant and oxidant, respectively. The E_a and λ values were determined from the Arrhenius plots of ln k vs $1/T$ (Figure 3, eq 1) and from the Marcus equation (eq 2), respectively.

As seen from Table 1, reorganization energies calculated for Pdx are consistent with those expected in biological ET reactions, 0.2−2.5 eV (*50*−*53*). In accord with the crystallographic data (*32*), the high λ value for the reductive step (2.3 eV) suggests that major nuclei, dipole, and charge rearrangements take place upon metal cluster reduction. All mutations led to a slight-to-moderate decrease (3−20%) of E_a, preexponential factor (A), and λ. Changes in the thermodynamic parameters did not correlate with the redox potential fluctuations caused by the mutations but were dependent on how far the altered residues were from the active site (Figure 2, Table 2). The largest effect was caused by elimination of the Trp106 aromatic ring, most likely due to increased solvent accessibility and polarizability of the [2Fe-2S] center. On the basis of these results we conclude that the 70−80% decrease in Pdr-to-Pdx ET rates owing to replacement of Tyr33, Asp38, or Arg66 observed previously (*33*) was due to perturbed protein−protein interactions and/or ET pathways and not due to changes in the intrinsic properties of Pdx.

The considerably lower E_a and λ values derived for Pdx oxidation (Table 1) indicate that the activation energy barrier for this reaction is lower than that for the reductive step. Another difference between the oxidation and reduction reactions was a more complex effect of the mutations on Pdx oxidation. Compared to WT, E_a and λ calculated for Y33F, R66A, and R66E Pdx were not significantly different while those determined for the Trp106 and Asp38 mutants decreased by 34−52%. Again, substitutions closest to the active site affected the thermodynamic parameters to a greater extent than those remote from the [2Fe-2S] center.

Effect of Mutations on the Electron Transfer to Ferric P450cam (ET1). Having established how mutations influence the electron-donating ability of Pdx, we next studied the effect of mutations on the two Pdx-to-P450cam ET processes. Since only the first ET from D38N, W106F, and Δ106 Pdx to P450cam has been investigated (*54*−*56*), we included these variants in our more comprehensive study. ET1 kinetics was studied by stopped-flow spectrophotometry and monitored at 446 nm, the maximum for the Fe^{2+}−CO complex of the hemoprotein (Figure 4A). The limiting k_{ET1} values

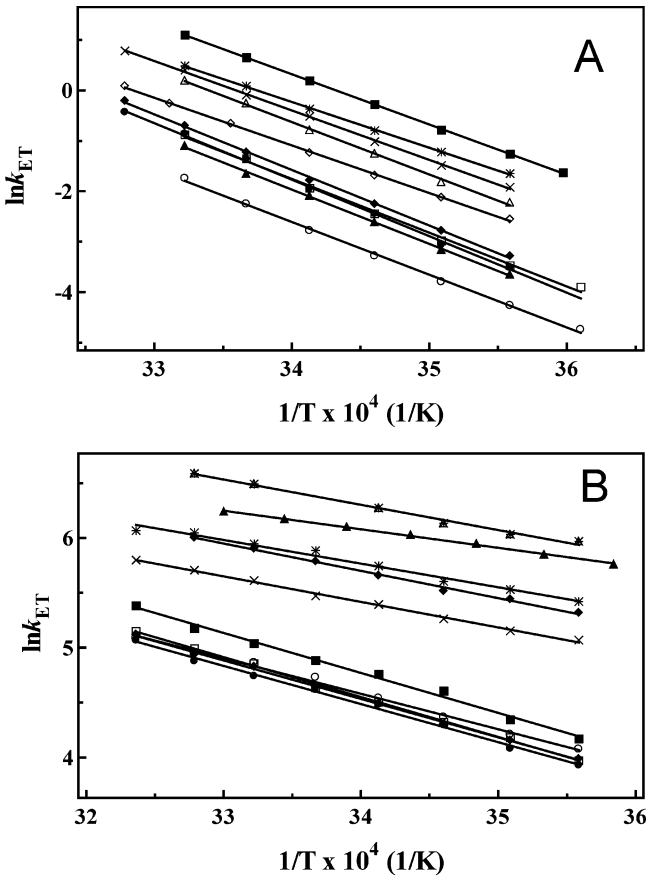

FIGURE 3: Thermodynamic analysis of the ET reactions to (A) and from (B) Pdx. Reduction and oxidation of WT (filled circle), Y33A (open circle), Y33F (filled square), D38A (filled triangle), D38N (open triangle), R66E (open square), R66A (filled diamond), Δ106 (open diamond), W106A (×), and W106F (*) with 5 mM sodium dithionite and 100 μM CoQ_0, respectively, were monitored under anaerobic conditions at 456 nm and 4 °C. The reaction buffer contained 50 mM phosphate, pH 7.5, and an oxygen-scrubbing system consisting of 1 mM glucose, 1 unit/mL catalase, 1 unit/mL glucose oxidase, and 40−50 μM Pdx. Prior to reaction with CoQ_0, Pdx was reduced using catalytic amounts of Pdr and subequimolar concentrations of NADH. The natural logarithms of the observed rate constants (k_{ET}) for the reduction and oxidation reactions were plotted against 1/*T*. Each point represents an average of at least three measurements. Solid lines are linear fits to the Arrhenius equation (eq 1). The derived thermodynamic parameters are given in Table 1.

(k_{cat}) and apparent dissociation constants (K_d) calculated from the hyperbolic fits to the plots of k_{ET1} vs [Pdx] are given in Table 2. Compared to WT Pdx, K_d's calculated for all of the mutants were 4−30-fold lower, indicating a decreased binding affinity for ferric P450cam (Table 2). In contrast, k_{cat} was affected by the mutations to different extents: Y33A, R66A, and R66E substitutions increased the maximal ET rate by 12−29%; W106F had no effect; Y33F and D38A substitutions led to a moderate decrease (15−20%); and D38N, W106A, and Δ106 mutations lowered k_{cat} by 80−85%. If any of these residues were comprising a specific ET pathway and hence were critical for the reduction process, one would expect much larger decreases in k_{cat}. Since the major effect of the mutations was on K_d, it is reasonable to conclude that the binding rather than the ET event between Pdx^r and ferric P450cam was predominantly altered and that the observed decreases in k_{cat} are due to improper orientation in the Pdx−P450cam complex which slows but does not shut down ET1. Asp38 and Trp106 were the most important for ET1 since mutations at these sites caused both an increase in K_d and the largest decrease in k_{cat}.

Effect of Mutations on the Electron Transfer to Oxy-P450cam (ET2). In sharp contrast to ET1, the various mutations introduced in Pdx had only a modest effect on K_d for oxy-P450cam with all except one leading to at most a 2-fold increase (Table 2). The one exception is the D38N substitution, which caused about a 3−4-fold increase in K_d, suggesting that, as in ET1, Asp38 is important for binding. The second dramatic difference between the two reductive steps was that the D38A, W106A, and Δ106 mutations led to >99% drop in ET2 k_{cat}. Taken together, the kinetic results indicate that (i) Asp38 and Trp106 are much more important in ET2 than in ET1 and (ii) the P450cam−Pdx^r complexes formed during the two reductive steps must be structurally different and/or use different ET paths.

Importantly, in contrast to earlier studies (*9*, *57*−*59*), our results and data reported recently by others show that ET2 is considerably faster than ET1 at any Pdx:P450cam ratio (*9*, *10*, *40*, *54*, *60*−*63*). This observation coupled with small differences in kinetic K_d values calculated for the Pdx^r−P450cam and Pdx^r−oxy-P450cam pairs, 2−15 (*40*, *63*, *64*) vs 4.4−23 μM (*40*, *60*), suggests that ET1 rather than ET2 is likely to limit the catalytic turnover in the native camphor-hydroxylating system.

Finally, the strikingly different effects of the Tyr33, Asp38, Arg66, and Trp106 substitutions on the ET to and from Pdx indicate that, in contrast to the Pdr−Pdx couple, where Tyr33 and Arg66 play the leading role in controlling the rate-limiting Pdx^r dissociation (*33*), Asp38 and Trp106 are the key residues that regulate binding and ET between Pdx^r and P450cam. Recruitment of distinct structural elements and the involvement of different regulating mechanisms during the Pdr−Pdx and P450cam−Pdx complex formation seem to be the factors that make protein−protein interactions in P450cam monooxygenase so highly specific.

Modeling Pdx−P450cam Interactions: Optimization of the Pochapsky Model. To better understand differences between the two P450cam reduction steps, we utilized a computer modeling approach and searched for plausible P450cam−Pdx orientations that would be in agreement with the experimental data. First, we tested if the complex proposed by Pochapsky and co-workers (*15*) is a suitable model for either ET1 or ET2. This complex was generated by manually bringing the 1PUT Pdx molecule into the proximal groove of P450cam to achieve the closest possible approach between the cofactors (12 Å) and to allow interaction between Arg79, Arg109, and Arg112 of P450cam and the C-terminal carboxyl, Asp34, and Asp38 of Pdx, respectively, because an important role of charged residues, in particular $Arg112_{P450}$, in P450cam−Pdx association had been suggested (*9*, *13*, *14*, *59*, *65*, *66*). To explain the stabilizing effect of $Trp106_{Pdx}$ on the interprotein complex formation and ET mediation (*5*, *54*, *55*, *67*), the C-terminal residue was placed close to $Tyr78_{P450}$ (ca. 6.0 Å away).

The validity of the Pochapsky model has been experimentally tested, and some but not all predictions have been confirmed (*56*, *60*, *68*). The major disadvantage of the complex, however, was the poorly refined 1PUT Pdx structure used for modeling. To optimize the model, we replaced 1PUT Pdx with the crystallographic molecule B of

Table 1: Thermodynamic Parameters for Electron Transfer Reactions Involving Putidaredoxin

	reduction by sodium dithionite				oxidation by CoQ_0			
	E_a[a] (kJ/mol) [%]	ln A[b]	$\Delta G°$[c] (kJ V^{-1} mol^{-1})	λ[d] (eV)	E_a (kJ/mol) [%]	ln A	$\Delta G°$ (kJ V^{-1} mol^{-1})	λ (eV)
WT	93.8 ± 1.5 [100]	36.6 ± 0.6	−42.2	2.30 ± 0.04	28.9 ± 0.1 [100]	16.3 ± 0.3	−33.0	0.79 ± 0.03
Y33A	89.2 ± 1.5 [95]	33.0 ± 0.6	−40.7	2.19 ± 0.04	26.8 ± 0.8 [93]	15.6 ± 0.3	−34.4	0.74 ± 0.02
Y33F	82.9 ± 0.4 [88]	34.2 ± 0.2	−40.1	2.05 ± 0.01	30.3 ± 1.0 [105]	17.2 ± 0.4	−35.0	0.83 ± 0.03
D38A	89.4 ± 1.4 [95]	34.6 ± 0.6	−40.0	2.19 ± 0.03	14.0 ± 0.3 [63][e]	11.8 ± 0.1	−35.1	0.49 ± 0.01
D38N	86.5 ± 1.9 [92]	34.8 ± 0.8	−39.8	2.13 ± 0.05	19.2 ± 0.8 [66]	14.2 ± 0.3	−35.4	0.49 ± 0.02
R66A	90.8 ± 1.3 [97]	36.0 ± 0.5	−41.5	2.23 ± 0.03	29.2 ± 0.5 [101]	16.5 ± 0.2	−33.7	0.80 ± 0.01
R66E	88.7 ± 2.3 [95]	34.5 ± 0.9	−41.5	2.18 ± 0.06	30.2 ± 0.6 [104]	16.9 ± 0.2	−33.7	0.83 ± 0.02
W106F	81.5 ± 1.0 [87]	32.9 ± 0.4	−41.8	2.03 ± 0.02	19.3 ± 0.4 [67]	13.3 ± 0.2	−33.4	0.51 ± 0.01
W106A	75.4 ± 0.8 [80]	30.6 ± 0.4	−39.6	1.88 ± 0.02	19.1 ± 0.7 [66]	13.6 ± 0.3	−35.6	0.48 ± 0.02
Δ106	78.6 ± 0.9 [84]	31.1 ± 0.4	−42.4	1.97 ± 0.02	20.7 ± 0.6 [72]	14.2 ± 0.3	−32.8	0.56 ± 0.02

[a] Activation energy was calculated from the Arrhenius plots (Figure 3). Standard deviations were derived from the linear fits to the plots. [b] The logarithm of the preexponential coefficient was calculated from the Arrhenius plots (Figure 3). Standard deviations were derived from the linear fits to the plots. [c] Free energy of the reaction was calculated from the $\Delta G° = -nF\Delta E_m$ equation, where n is the number of electrons transferred during the reaction, F is the Faraday constant, and ΔE_m is the difference between redox potentials of an electron donor and acceptor. [d] Apparent reorganization energy was calculated from the Marcus equation $E_a = (\lambda + \Delta G°)^2/4\lambda$. [e] Measured under different conditions as described in Experimental Procedures.

Table 2: Redox Properties of the Wild-Type Pdx and Mutants of Pdx

		first ET to P450cam		second ET to P450cam	
Pdx	$E_{1/2}$[a] (mV vs SHE)	k_{cat} (s^{-1}) (25 °C) [%]	K_d (μM)	k_{cat} (s^{-1}) (4 °C) [%]	K_d (μM)
WT	−162	41 ± 1 [100]	7 ± 1	118 ± 10 [100]	23 ± 4
Y33A	−177	46 ± 9 [112]	218 ± 25	55 ± 1 [47]	43 ± 1
Y33F	−183	33 ± 2 [80]	83 ± 11	64 ± 9 [54]	49 ± 8
D38A	−184	35 ± 3 [85]	198 ± 20	0.33 ± 0.05 [<1]	31 ± 9
D38N	−187	9 ± 1 [22]	117 ± 9	21 ± 1 [18]	86 ± 6
R66A	−169	53 ± 4 [129]	143 ± 16	62 ± 3 [53]	27 ± 3
R66E	−169	47 ± 3 [115]	41 ± 7	42 ± 4 [36]	41 ± 7
W106F	−166	41 ± 2 [100]	29 ± 3	71 ± 7 [60]	23 ± 5
W106A	−189	6 ± 1 [15]	108 ± 15	0.11 ± 0.01 [<1]	29 ± 2
Δ106	−160	9 ± 1 [22]	163 ± 18	0.32 ± 0.03 [<1]	46 ± 8

[a] Determined previously by cyclic voltammetry (*33*).

reduced C73S Pdx (PDB code 1XLQ), pulled it 3.0 Å away to eliminate clashing with P450cam, adjusted side chains of the interface residues, and energy minimized the resulting structure that will be referred to as model 1. Molecule B of 1XLQ Pdx was chosen because it undergoes the largest conformational change upon [2Fe-2S] reduction (*32*). Structural overlay of the original and optimized complexes is shown in Figure 5A. Owing to an increased Fe−Fe distance, protein−protein interactions observed in model 1 were somewhat different from those in the original complex: $Arg109_{P450}$−$Trp106_{Pdx}$−COOH and $Arg112_{P450}$−$Asp38_{Pdx}$ salt bridges were preserved, $Arg109_{P450}$−$Asp34_{Pdx}$ and $Arg79_{P450cam}$−$Trp106_{Pdx}$-COOH pairs disrupted, and new $Glu286_{P450}$−$Arg66_{Pdx}$ and $Lys344_{P450}$−$Glu65_{Pdx}$ charge−charge interactions formed (Table 3). This agrees well with the experimental data showing that $Arg109_{P450}$ is important for P450cam−Pdx association (*11*, *68*) while $Arg79_{P450}$ and $Asp34_{Pdx}$ are not (*56*, *60*). A salt bridge between $Glu65_{Pdx}$ and $Lys344_{P450}$, proven to be not essential for the activity of the redox couple (*13*, *64*), is situated at the edge of interface and thus may not have a significant impact on a long-range stirring of productive collisions between the proteins. Importantly, the indole ring of Trp106 in model 1 is sandwiched between the Cys45−Thr47 part of the metal-binding loop of Pdx and the aliphatic side chain of $Leu356_{P450}$. These hydrophobic interactions are more extensive than in the original model and better explain the important role of Trp106 in the P450cam binding and ET mediation processes (*5*, *54*, *55*, *67*).

Depending on whether single iron atoms or the entire cofactor groups were chosen as an electron donor/acceptor, theoretical calculations predicted two different ET pathways (Figure 5B, Table 4): the Fe-to-Fe route included the iron−sulfur cluster ligand Cys45 and the Leu356-Cys357 peptide of P450cam, whereas the [2Fe-2S]-to-heme path proceeded from $Cys39_{Pdx}$ through the main and side chain atoms of $Asp38_{Pdx}$ to a heme propionate via $Arg112_{P450}$. Establishment of the $Asp38_{Pdx}$−$Arg112_{P450}$ salt bridge in the P450cam−Pdx ET complex has been widely anticipated (*11*, *66*, *68*, *69*). Since shortening of the Asp38 side chain to Ala has a moderate effect on ET1 and drastically diminished ET2 (Table 2), we conclude that the optimized Pochapsky complex can be considered as a plausible model for the first but not the second ET process. Furthermore, since the L356A replacement had no effect on P450cam activity (*70*), we suggest that the $Cys39_{Pdx}$−$Asp38_{Pdx}$−$Arg112_{P450}$ route is predominant during ET1 but not unique. Considerably higher values of theoretically predicted ET rates relative to those measured experimentally suggest that the conformation observed in model 1 may not be easily achieved in solution and a dynamic motion between the proteins (conformational gating) may be required before the actual ET occurs.

Screening for Other Possible P450cam−Pdx Conformations. In order to find an orientation between P450cam and Pdx that would be in agreement with the ET2 kinetics, we utilized the program GRAMM that performs an exhaustive computational search of all possible configurations to find complexes with the highest surface complementarity (*41*).

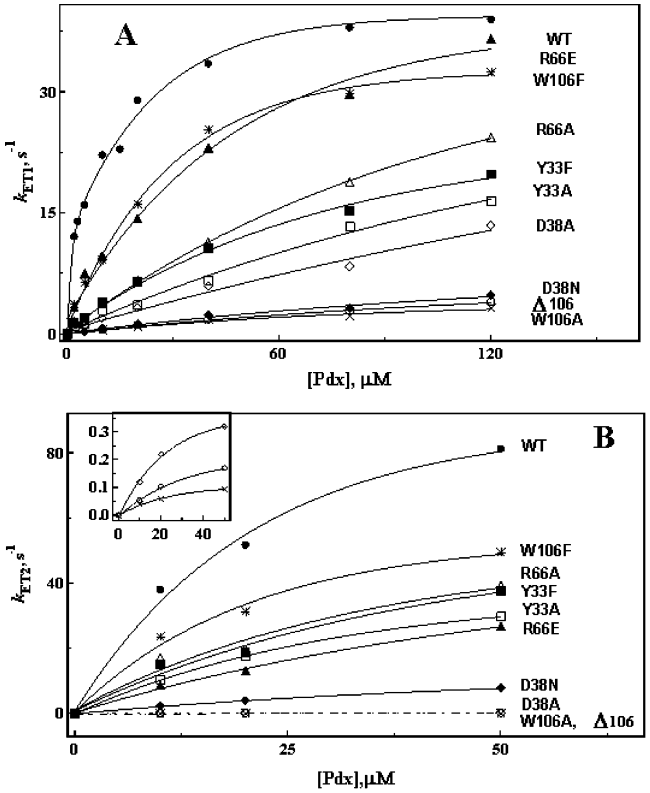

FIGURE 4: Plots of the observed ET rate constants vs [Pdx] for the transfer of an electron from Pdx^r to ferric (A) and oxy-P450cam (B). Reduction of 2 μM ferric P450cam with various concentrations of Pdx^r was monitored at 446 nm and 25 °C to follow formation of the ferrous−CO form in carbon monoxide saturated 50 mM phosphate buffer, pH 7.5, containing 100 mM KCl, 1 mM camphor, and an oxygen-scrubbing system. ET from Pdx^r to oxy-P450cam was measured at 390 nm and 4 °C using a sequential double mixing mode of the stopped-flow spectrophotometer to follow decomposition of oxy-P450cam into ferric enzyme and hydroxycamphor. The k_{cat} and K_d values for the reactions were determined from the hyperbolic fits shown in solid lines. Inset B is a zoomed in view at the k_{ET2} vs [Pdx] plots for the D38A (open diamond), W106A (×), and Δ106 mutants (open circle).

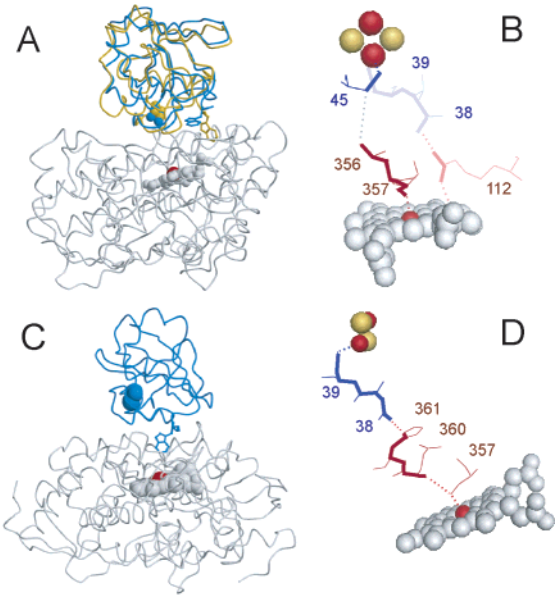

FIGURE 5: Models of the P450cam−Pdx ET complexes. (A) Superposition of the original [1PUT Pdx^o in gold (*15*)] and optimized Pochapsky models (model 1, molecule B of 1XLQ Pdx^r in blue). (B) Two Pdx^r-to-P450cam ET pathways (highlighted in bold lines) predicted for model 1 by HARLEM (*45*) depending on whether single iron atoms or the entire cofactor groups were chosen as an electron donor/acceptor. The Fe-to-Fe route, shown in dark blue and brick colors, follows from the iron−sulfur cluster to the Cys45 ligand and via space jump to the Leu356-Cys357 peptide of P450cam. The [2Fe-2S]-to-heme path, shown in light blue and pink colors, proceeds from the [2Fe-2S] ligand Cys39 through the main and side chain atoms of Asp38 and via the Asp38−Arg112$_{P450}$ and Arg112$_{P450}$−propionate hydrogen bonds to the heme group. (C) An optimized oxy-P450cam−Pdx^r complex generated by GRAMM (model 2, Pdx shown in blue). (D) The unique ET root predicted for model 2 by HARLEM follows from the [2Fe-2S] cluster through the Cys39$_{Pdx}$-Asp38$_{Pdx}$ and His361$_{P450}$-Gln360$_{P450}$ peptides and the Asp38$_{Pdx}$−His361$_{P450}$ and Glu360$_{P450}$−Cys357$_{P45O}$ hydrogen bonds to the heme cofactor.

The initial stage of interprotein ET reactions is a translational and rotational diffusion of protein pairs to form associated complexes, a process influenced by electrostatic and static forces communicated through the solvent electrolyte medium. Owing to a small dipole moment and the mostly neutral active site of the Pdx molecule (*34*), it is likely that surface complementarity rather than electrostatic steering between P450cam and Pdx will guide the first recognition step. In this regard, GRAMM was a suitable program for identifying docking regions in the P450cam−Pdx couple, and, as we found, it detected a few "hot" spots on the surface of the hemoprotein where Pdx could preferably bind. Importantly, the docking pattern, shown in detail in the Supporting Information (Figures S1−S4), suggested that the P450cam−Pdx association in solution might be guided/controlled not only by the redox state of Pdx (*71*, *72*) but also by redox-linked conformational changes in P450cam.

Conformational Dynamics in P450cam. To understand how the redox state of P450cam could affect Pdx recognition, we compared crystal structures of ferric and oxy-P450cam (*35*, *42*) and found that binding of dioxygen to the heme iron causes small but noticeable changes on the proximal face of P450. To accommodate O_2 and a catalytically important water molecule in the oxygen-binding groove (Wat234, Figure 6A), the Asp251-Thr252 peptide in the central I helix undergoes a conformational change. As a result, the groove widens by ca. 0.7 Å, Thr252 moves aside and establishes hydrogen bonds with the ligand and water molecules, and the I helix straightens (Figure 6B). Through the adjacent and neighboring I−H loop and helices E and J, movement in the I helix transmits to helices C, D, H, and K that constrict around the hydrophobic pocket and make it more pronounced (Figure 6C). These redox-linked changes in surface properties of P450cam, that are likely to be more dramatic in the soluble protein, could facilitate not only recognition and selective binding of one redox form of Pdx over another but also assist in Pdx^o dissociation when ET is completed.

Modeling the Second Electron-Transfer Step. Four out of 50 top-ranked oxy-P450cam−Pdx^r complexes predicted by GRAMM had a plausible geometry with the Fe−Fe distance less than 20 Å (Figure 7), the limiting distance for the interprotein ET to occur at physiologically relevant rates (*73*). In one of these complexes, Pdx was docked in such a way that its C-terminal Trp106, proven to exhibit conformational freedom in both oxidized and reduced Pdx (*67*), was positioned above the proximal groove (solution 49, Figure 7). After optimization, the complex was energy minimized

Table 3: Comparison of Model P450cam−Pdx Complexes

	model 1		model 2	
	P450cam	Pdx	P450cam	Pdx
E_{total} (kcal/mol)[a]	18736		18507	
area of interface (Å^2)	143		284	
salt bridge interactions	Arg109	Trp106 carboxyl	Glu76	Arg104
	Arg112	Asp38	Arg109	Asp103
	Glu286	Arg66	Arg364	Asp38
	Lys344	Glu65		
hydrogen-bonding interactions	Val345 (O)	Arg66(Nξ)	Glu117 (Oϵ)	Gly31 (O)
	His361 (Nϵ)	Asp38 (O)	His361 (Nδ)	Asp38 (Oδ)
	Arg364 (Nξ)	Ser42 (Oγ)	Gln117 (Oϵ)	Arg113 (Nξ)[b]
			Asp125 (Oδ)	Ser29 (Oγ)[b]
			Asn229 (Nδ)	Asp9 (Oδ)[b]
van der Waals contacts (bond length 2.8−4.0 Å)	His361	Cys39	Asn116	Tyr33
			Met121	Val36, Gly37
			Pro122	Val28
			His361	Val28
			His347, Gln360, Arg364	Trp106
hydrophobic interactions	Met121	Val28	Met121	Val28
	Leu356	Trp106	Phe350, Leu356	Trp106
			Ala113	Tyr33

[a] Total energy of the minimized models. [b] Potential water-bridged H-bonding interactions.

Table 4: Electronic Coupling, Pathways, and ET Rates Calculated for the Model Pdx−P450cam Complexes Using the Program HARLEM

	model 1		model 2	
[2Fe-2S]−heme distance (Å)[a]	15.0		18.7	
donor−acceptor	$Fe1_{Pdx}$−Fe_{P450}	[2Fe-2S]−heme	$Fe1_{Pdx}$−Fe_{P450}	[2Fe-2S]−heme
electronic coupling (H_{AB})[b]	4.0×10^{-5}	1.34×10^{-5}	2.0×10^{-6}	2.0×10^{-6}
atom packing density (ρ)[c]	0.77	0.68	0.74	0.67
av decay exponential (β) (Å^{-1})[d]	1.35	1.51	1.40	1.53
electron pathway[e]	$Fe1_{Pdx}$−$C^{45}{}_{Pdx}$→ $L^{356}{}_{P450}$−$C^{357}{}_{P450}$−Fe_{P450}	$Fe1_{Pdx}$−$C^{39}{}_{Pdx}$−$D^{38}{}_{Pdx}$→ $R^{112}{}_{P450}$−heme	$Fe1_{Pdx}$−$C^{39}{}_{Pdx}$−$D^{38}{}_{Pdx}$→ $H^{361}{}_{P450}$−$Q^{360}{}_{P450}$−$C^{357}{}_{P450}$−Fe_{P450}	same
max electron transfer rate (s^{-1})[f]	1.6×10^5	1.8×10^4	422	35

[a] Distance between the Fe1 atom of [2Fe-2S] and the heme iron. [b] H_{AB} is the electronic tunneling coupling matrix element that describes the degree of wave function overlap occurring between the donor and acceptor. [c] ρ is the fraction of sampled space between atoms of redox cofactors that fall inside the van der Waals radii of the protein atoms. [d] β is a parameter in the term $e^{-\beta R}$ that represents the exponential falloff of the electronic tunneling rate with distance. [e] Atoms and residues predicted to provide the most efficient electron transfer path from the [2Fe-2S] cluster to the heme. [f] Maximum electron transfer rate predicted for this particular electron pathway.

and designated as model 2 (Figure 5C), structural and electronic characteristics of which are given in Tables 3 and 4. As seen from Figure 5A,C, switching between Pdx^r positions in the complexes with ferric and oxy-P450cam (models 1 and 2, respectively) can be achieved by ca. 50° rotation around the axis perpendicular to the display. As a result, the side of the Pdx molecule rather than the active site area provides the majority of interactions with P450cam in model 2. In addition, in this complex (i) the interface becomes two times larger with more intermolecular contacts, (ii) Trp106 forms extensive hydrophobic and van der Waals contacts with the residues comprising the heme-binding loop, (iii) the side chain of Tyr33 is buried at the interface in a mainly nonpolar environment, and (iv) Asp38 establishes ionic and H-bonding interactions with Arg364 and His361 of P450cam (Table 3). Involvement of $His361_{P450}$ in redox partner recognition has not yet been tested, whereas the R364C replacement was shown to result in ca. 30% decrease in monooxygenase activity (*69*).

In contrast to model 1, $Arg112_{P450}$ did not form direct contacts with any Pdx residue and therefore was not predicted to be a part of the ET route. According to the theoretical calculations, the Fe-to-Fe and [2Fe-2S]-to-heme pathways predicted for model 2 were identical and included the $Cys39_{Pdx}$-$Asp38_{Pdx}$ and $His361_{P450}$-$Gln360_{P450}$ peptides, the heme ligating $Cys357_{P450}$, and two hydrogen bonds, $Asp38_{Pdx}$-(Oδ)−$His361_{P450}$(Nδ) and $Glu360_{P450}$(N)−$Cys357_{P450}$(S) (Figure 5D, Table 4). Owing to a longer distance between the redox groups (18.7 vs 15.0 Å in model 1), maximum ET rates predicted for this route were 2−3 orders of magnitude lower and close to those measured experimentally.

Comparison of the theoretical and experimental data shows that model 2 explains the second ET step rather well. First, in agreement with our kinetic data (Table 2), model 2 suggests that a residue at position 38 must have a negatively charged side chain to optimally orient Pdx and, most importantly, provide media for a unique ET pathway. Second, according to the model, tryptophan is required at position 106 because only the bulky, rigid indole ring can penetrate into the proximal groove deep enough to push the heme-binding loop, Cys357−His361, and modulate the electronic structure of the heme−thiolate complex, shown to be necessary for acceleration of the O−O bond scission and product formation (*18*, *19*). The potential "pushing" ability of Trp106 could explain in part the effector role of Pdx in P450cam catalysis (*3*, *5*, *6*). Third, model 2 explains why the Tyr33 variants have a lower capability to bind and reduce oxy-P450cam. Extensive hydrophobic interactions established by Trp106 need to be disrupted upon Pdx oxidation, and redox-linked movements of the buried Tyr33 side chain

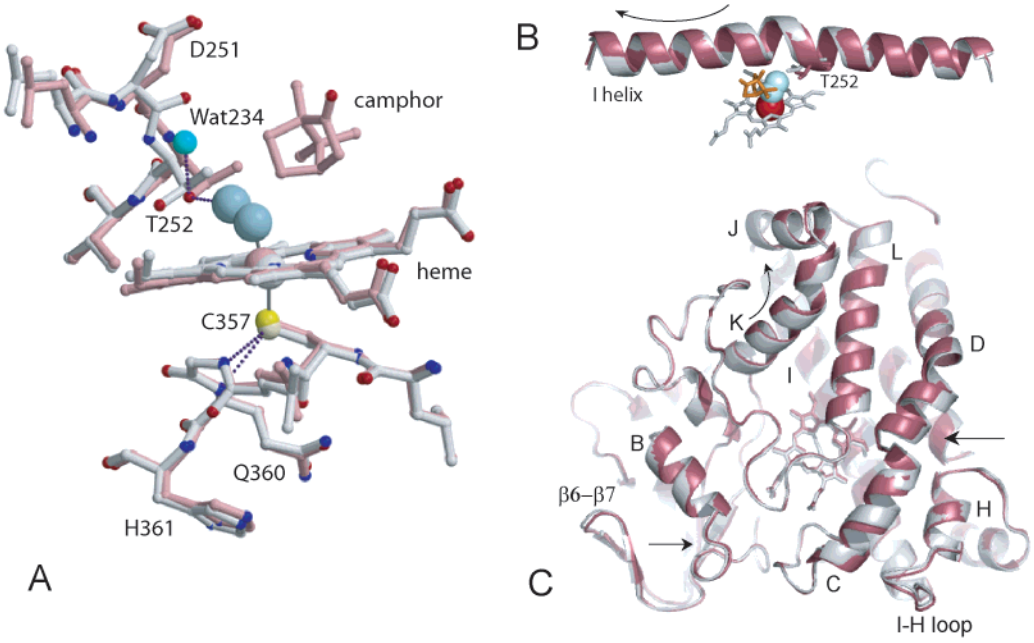

FIGURE 6: Structural changes in the active site (A), the I helix (B), and the proximal face (C) of P450cam induced by one-electron reduction and dioxygen binding. Superposition of the crystal structures of ferric [gray (*42*)] and oxy-P450cam [pink, maroon (*35*)] was performed using the program LSQMAN (*78*). The O_2 and catalytically important water molecules are shown in blue. Rearrangements in the oxygen-binding groove and the I helix transmit via adjacent and neighboring helices E and J and an H−I loop to helices C, D, H, and K that constrict around the hydrophobic pocket and make it more pronounced. Arrows show redox-linked movements of structural elements.

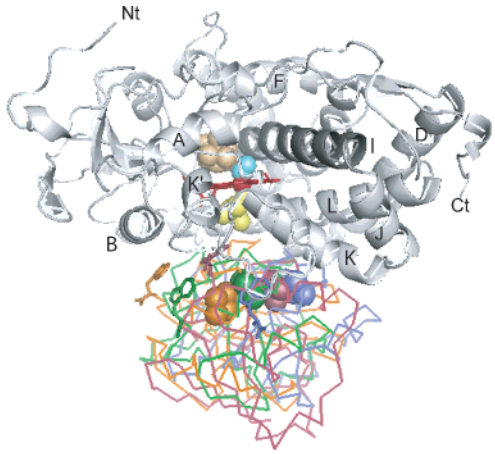

FIGURE 7: Four plausible orientations between oxy-P450cam (gray) and Pdx^r corresponding to solutions 4, 28, 46, and 49 generated by GRAMM (blue, green, orange, and maroon, respectively) where the Fe−Fe distance is less than 20 Å. The helix designation in P450cam is according to Poulos et al. (*79*) with the functionally important I helix highlighted in dark gray. The heme iron (red), camphor (beige), dioxygen (cyan), and the iron-ligating Cys357 (yellow) in P450cam and the [2Fe-2S] cofactors in Pdx are in CPK representation.

(*32*) could assist dissociation and ensure fast turnover. Fourth, the model complex helps to understand why substitutions of Arg112$_{P450}$, which do not form direct contacts with Pdx, inhibit ET2 (*10*, *60*). A functionally important Arg112 provides hydrogen bonds to the heme propionate, defines the conformation of the heme-binding loop, regulates the redox potential and the spin state of the heme iron, and participates in redox partner recognition (*10*, *14*, *60*, *66*, *69*). This arginine is situated 4.5 Å away from another basic surface residue, Arg109, that was demonstrated to be crucial for both P450cam−Pdx^r and oxy-P450cam−Pdx^r association (*60*). In accord with these experimental data, Arg109 forms electrostatic interactions with the C-terminal carboxyl and Asp103 of Pdx in models 1 and 2, respectively (Table 3), and thus is predicted to be important for both ET1 and ET2 complex formations. On the basis of the theoretical predictions and the proximity of Arg109 to Arg112, we postulate that the latter residue might assist P450cam−Pdx interaction indirectly by repulsing and directing the Arg109 side chain into the solvent toward the redox partner.

Since Arg66 is not a part of the protein−protein interface in model 2 and is ca. 12 Å away from the nearest P450cam residue, the inhibiting effect of Arg66 mutations on the ET2 rates (Table 2) can be due to changes in the overall electrostatic properties of Pdx which could alter the initial recognition step and prevent achieving an optimal orientation for ET2. Although the R66A/E replacements slightly increase reorganization energy for the Pdx oxidation reaction (Table 1), their significant effect on the intrinsic properties of Pdx can be ruled out because neither variant perturbs the ET1 process.

The Effector Role of Pdx. In addition to the pushing ability of Trp106 derived from model 2, our modeling results reveal another possibility for the coupling effector action of Pdx. Since there is physical evidence that aggregates with the 1:3 and 1:6 P450cam:Pdx ratios can be formed in solution (*74*) and that complex formation with Pdx induces structural changes in both the proximal side (*17*, *20*) and the distal pocket of P450cam (*17*, *75*, *76*), it is possible that the redox-controlled selective binding between the redox partners detected by GRAMM (Figures S1−S4) is functionally important. The preferred docking of Pdx^o near the substrate access channel and along the sides of P450cam could regulate positioning of camphor, help to stabilize the I helix in an energetically strained conformation essential for catalysis, and increase Pdx^r chances to find the ET site before it loses

an electron. This suggestion agrees in part with the NMR data (*23*, *24*) showing that Pdx^r causes structural perturbations not only at the proximal side of ferrous CO-bound P450cam but also in the remote areas, in particular, around two sites predicted by GRAMM (Figures S1−S4). On the basis of these observations it was concluded that the primary effector role of Pdx is to enforce P450cam conformations that prevent dissociation of substrate/intermediates from the active site prior to turnover and to assist proton/electron coupling. Notably, Rui et al. found that the binding sites for cytochrome b_5, a nonphysiological effector of P450cam monooxygenase (*3*, *6*), overlapped with those detected for Pdx^r but were less specific (*24*). As a control experiment, we analyzed possible docking positions between the ferric and oxy forms of P450cam and cytochrome b_5. In accord with the magnetic resonance and the binding competition studies (*77*), the docking patterns predicted for Pdx and cytochrome b_5 had some degree of overlap (Figures S5 and S6). Unlike the P450cam−Pdx pair, however, none of the top-scored P450cam−cytochrome b_5 complexes had the effector molecule bound to the proximal groove. This implies that cytochrome b_5 does not have the correct structure to fit into the active site and explains why cytochrome b_5 binding has only a minor effect on the P450cam heme environment (*20*) and its considerably larger excess over Pdx is needed to achieve a similar coupling effect on the camphor hydroxylation reaction (*6*).

Conclusions. The results presented in this study show that reduction of ferric (ET1) and oxy-P450cam (ET2) involves formation of different complexes with Pdx^r and/or different electron transfer paths. Specific mutations introduced in Pdx have different effects on the two reductive steps, indicating that Asp38 and Trp106 are much more important in ET2 than in ET1. Computer-generated models of the P450cam−Pdx^r and oxy-P450cam−Pdx^r complexes are consistent with the experimental results and allow to conclude that one of the reasons that Pdx can act as an effector and couple ET2 to camphor hydroxylation is that its C-terminal Trp106 can approach the heme-binding loop on the proximal surface of P450cam closely enough to modulate the electronic structure of the heme−thiolate complex. Computer modeling also suggests that P450cam−Pdx interaction can be controlled by the redox state of both proteins. This and the potential ability of Pdx to bind in the areas remote from the proximal side and regulate different steps of the monooxygenation reaction explain why Pdx is the most potent effector in the P450cam catalysis.

ACKNOWLEDGMENT

The authors thank T. C. Pochapsky for providing coordinates of the model P450cam−Pdx complex.

SUPPORTING INFORMATION AVAILABLE

Top-scored P450cam−Pdx^o (Figure S1), P450cam−Pdx^r (Figure S2), oxy-P450cam−Pdx^o (Figure S3), oxy-P450cam−Pdx^r (Figure S4), P450cam−cyt b_5 (Figure S5), and oxy-P450cam−cyt b_5 complexes (Figure S6) predicted by GRAMM. This material is available free of charge via the Internet at http://pubs.acs.org.

REFERENCES

1. Katagiri, M., Ganguli, B. N., and Gunsalus, I. C. (1968) A soluble cytochrome P450 functional in methylene hydroxylation, *J. Biol. Chem. 243*, 3543−3546.
2. Tsai, R. L., Gunsalus, I. C., and Dus, K. (1971) Composition and structure of camphor hydroxylase components and homology between putidaredoxin and adrenodoxin, *Biochem. Biophys. Res. Commun. 45*, 1300−1306.
3. Tyson, C. A., Lipscomb, J. D., and Gunsalus, I. C. (1972) The role of putidaredoxin and P450cam in methylene hydroxylation, *J. Biol. Chem. 247*, 5777−5784.
4. Geren, L., Tuls, J., O'Brien, P., Millett, F., and Peterson, J. A. (1986) The involvement of carboxylate groups of putidaredoxin in the reaction with putidaredoxin reductase, *J. Biol. Chem. 261*, 15491−15495.
5. Sligar, S. G., Debrunner, P. G., Lipscomb, J. D., Namtvedt, M. J., and Gunsalus, I. C. (1974) A role of the putidaredoxin COOH-terminus in P450cam (cytochrome m) hydroxylations, *Proc. Natl. Acad. Sci. U.S.A. 71*, 3906−3910.
6. Lipscomb, J. D., Sligar, S. G., Namtvedt, M. J., and Gunsalus, I. C. (1976) Autooxidation and hydroxylation reactions of oxygenated cytochrome P450cam, *J. Biol. Chem. 251*, 1116−1124.
7. Sligar, S. G. (1975) A kinetic and equilibrium description of camphor hydroxylation by the P450cam monooxygenase system, Ph.D. Thesis, University of Illinois, Urbana.
8. Hoa, G. H., Begard, E., Debey, P., and Gunsalus, I. C. (1978) Two univalent electron transfers from putidaredoxin to bacterial cytochrome P450 at subzero temperature, *Biochemistry 17*, 2835−2839.
9. Brewer, C. B., and Peterson, J. A. (1988) Single turnover kinetics of the reaction between oxycytochrome P450cam and reduced putidaredoxin, *J. Biol. Chem. 263*, 791−798.
10. Unno, M., Shimada, H., Toba, Y., Makino, R., and Ishimura, Y. (1996) Role of Arg112 of cytochrome P450cam in the electron transfer from reduced putidaredoxin. Analyses with site-directed mutants, *J. Biol. Chem. 271*, 17869−17874.
11. Shimada, H., Nagano, S., Hori, H., and Ishimura, Y. (2001) Putidaredoxin-cytochrome P450cam interaction, *J. Inorg. Biochem. 83*, 255−260.
12. Mueller, E. J., Loida, P. J., and Sligar, S. G. (1995) Twenty-five years of P450cam Research, in *Cytochrome P450: Structure, Mechanism, and Biochemistry* (Montellano, P. R. O. d., Ed.) 2nd ed., pp 83−125, Plenum Press, New York.
13. Stayton, P. S., and Sligar, S. G. (1990) The cytochrome P450cam binding surface as defined by site-directed mutagenesis and electrostatic modeling, *Biochemistry 29*, 7381−7386.
14. Koga, H., Sagara, Y., Yaoi, T., Tsujimura, M., Nakamura, K., Sekimizu, K., Makino, R., Shimada, H., Ishimura, Y., Yura, K., et al. (1993) Essential role of the Arg112 residue of cytochrome P450cam for electron transfer from reduced putidaredoxin, *FEBS Lett. 331*, 109−113.
15. Pochapsky, T. C., Lyons, T. A., Kazanis, S., Arakaki, T., and Ratnaswamy, G. (1996) A structure-based model for cytochrome P450cam-putidaredoxin interactions, *Biochimie 78*, 723−733.
16. Shaik, S., Kumar, D., de Visser, S. P., Altun, A., and Thiel, W. (2005) Theoretical perspective on the structure and mechanism of cytochrome P450 enzymes, *Chem. Rev. 105*, 2279−2328.
17. Unno, M., Christian, J. F., Benson, D. E., Gerber, N. C., Sligar, S. G., and Champion, P. M. (1997) Resonance Raman investigations of cytochrome P450cam complexed with putidaredoxin, *J. Am. Chem. Soc. 119*, 6614−6620.
18. Yoshioka, S., Takahashi, S., Ishimori, K., and Morishima, I. (2000) Roles of the axial push effect in cytochrome P450cam studied with the site-directed mutagenesis at the heme proximal site, *J. Inorg. Biochem. 81*, 141−151.
19. Yoshioka, S., Tosha, T., Takahashi, S., Ishimori, K., Hori, H., and Morishima, I. (2002) Roles of the proximal hydrogen bonding network in cytochrome P450cam-catalyzed oxygenation, *J. Am. Chem. Soc. 124*, 14571−14579.
20. Unno, M., Christian, J. F., Sjodin, T., Benson, D. E., Macdonald, I. D., Sligar, S. G., and Champion, P. M. (2002) Complex formation of cytochrome P450cam with putidaredoxin. Evidence for protein-specific interactions involving the proximal thiolate ligand, *J. Biol. Chem. 277*, 2547−2553.
21. Tosha, T., Yoshioka, S., Ishimori, K., and Morishima, I. (2004) L358P mutation on cytochrome P450cam simulates structural changes upon putidaredoxin binding: the structural changes trigger

electron transfer to oxy-P450cam from electron donors, *J. Biol. Chem. 279*, 42836−42843.
22. Nagano, S., Tosha, T., Ishimori, K., Morishima, I., and Poulos, T. L. (2004) Crystal structure of the cytochrome P450cam mutant that exhibits the same spectral perturbations induced by putidaredoxin binding, *J. Biol. Chem. 279*, 42844−42849.
23. Pochapsky, S. S., Pochapsky, T. C., and Wei, J. W. (2003) A model for effector activity in a highly specific biological electron transfer complex: The cytochrome P450cam-putidaredoxin couple, *Biochemistry 42*, 5649−5656.
24. Rui, L., Pochapsky, S. S., and Pochapsky, T. C. (2006) Comparison of the complexes formed by cytochrome P450cam with cytochrome b_5 and putidaredoxin, two effectors of camphor hydroxylase activity, *Biochemistry 45*, 3887−3897.
25. Pochapsky, T. C., Ye, X. M., Ratnaswamy, G., and Lyons, T. A. (1994) An NMR-derived model for the solution structure of oxidized putidaredoxin, a 2Fe-2S ferredoxin from Pseudomonas, *Biochemistry 33*, 6424−6432.
26. Sevrioukova, I. F., Garcia, C., Li, H., Bhaskar, B., and Poulos, T. L. (2003) Crystal structure of putidaredoxin, the [2Fe-2S] component of the P450cam monooxygenase system from *Pseudomonas putida*, *J. Mol. Biol. 333*, 377−392.
27. Smith, N., Mayhew, M., Holden, M. J., Kelly, H., Robinson, H., Heroux, A., Vilker, V. L., and Gallagher, D. T. (2004) Structure of C73G putidaredoxin from *Pseudomonas putida*, *Acta Crystallogr., Sect. D: Biol. Crystallogr. 60*, 816−822.
28. Jain, N. U., Tjioe, E., Savidor, A., and Boulie, J. (2005) Redox-dependent structural differences in putidaredoxin derived from homologous structure refinement via residual dipolar couplings, *Biochemistry 44*, 9067−9078.
29. Jain, N. U., and Pochapsky, T. C. (1998) Redox dependence of hyperfine-shifted ^{13}C and ^{15}N resonances in putidaredoxin, *J. Am. Chem. Soc. 120*, 12984−12985.
30. Sari, N., Holden, M. J., Mayhew, M. P., Vilker, V. L., and Coxon, B. (1999) Comparison of backbone dynamics of oxidized and reduced putidaredoxin by ^{15}N NMR relaxation measurements, *Biochemistry 38*, 9862−9871.
31. Pochapsky, T. C., Kostic, M., Jain, N., and Pejchal, R. (2001) Redox-dependent conformational selection in a $Cys_4Fe_2S_2$ ferredoxin, *Biochemistry 40*, 5602−5614.
32. Sevrioukova, I. F. (2005) Redox-dependent structural reorganization in putidaredoxin, a vertebrate-type [2Fe-2S] ferredoxin from *Pseudomonas putida*, *J. Mol. Biol. 347*, 607−621.
33. Kuznetsov, V. Y., Blair, E., Farmer, P. J., Poulos, T. L., Pifferitti, A., and Sevrioukova, I. F. (2005) The putidaredoxin reductase-putidaredoxin electron transfer complex: theoretical and experimental studies, *J. Biol. Chem. 280*, 16135−16142.
34. Sevrioukova, I. F., Li, H., and Poulos, T. L. (2004) Crystal structure of putidaredoxin reductase from *Pseudomonas putida*, the final structural component of the cytochrome P450cam monooxygenase, *J. Mol. Biol. 336*, 889−902.
35. Nagano, S., and Poulos, T. L. (2005) Crystallographic study on the dioxygen complex of wild-type and mutant cytochrome P450cam. Implications for the dioxygen activation mechanism, *J. Biol. Chem. 280*, 31659−31663.
36. Gunsalus, I. C., and Wagner, G. C. (1978) Bacterial P450cam methylene monooxygenase components: cytochrome m, putidaredoxin, and putidaredoxin reductase, *Methods Enzymol. 52*, 166−188.
37. Sevrioukova, I. F., and Poulos, T. L. (2002) Putidaredoxin reductase: A new function for an old protein, *J. Biol. Chem. 277*, 25831−25839.
38. Mayhew, S. G. (1978) The redox potential of dithionite and SO^{-2} from equilibrium reactions with flavodoxins, methyl viologen and hydrogen plus hydrogenase, *Eur. J. Biochem. 85*, 535−547.
39. Reipa, V., Holden, M. J., Mayhew, M. P., and Vilker, V. L. (2000) Temperature dependence of the formal reduction potential of putidaredoxin, *Biochim. Biophys. Acta 1459*, 1−9.
40. Tosha, T., Yoshioka, S., Hori, H., Takahashi, S., Ishimori, K., and Morishima, I. (2002) Molecular mechanism of the electron transfer reaction in cytochrome P450cam-putidaredoxin: roles of glutamine 360 at the heme proximal site, *Biochemistry 41*, 13883−13893.
41. Vakser, I. A., and Aflalo, C. (1994) Hydrophobic docking—a proposed enhancement to molecular recognition techniques, *Proteins 20*, 320−329.
42. Schlichting, I., Berendzen, J., Chu, K., Stock, A. M., Maves, S. A., Benson, D. E., Sweet, R. M., Ringe, D., Petsko, G. A., and Sligar, S. G. (2000) The catalytic pathway of cytochrome P450cam at atomic resolution, *Science 287*, 1615−1622.
43. Jones, T. A., Zou, J. Y., Cowan, S. W., and Kjeldgaard, M. (1991) Improved methods for building protein models in electron density maps and the location of errors in these models, *Acta Crystallogr. A 47*, 110−119.
44. Brunger, A. T., Adams, P. D., Clore, G. M., DeLano, W. L., Gros, P., GrosseKunstleve, R. W., Jiang, J. S., Kuszewski, J., Nilges, M., Pannu, N. S., Read, R. J., Rice, L. M., Simonson, T., and Warren, G. L. (1998) Crystallography + NMR system: A new software suite for macromolecular structure determination, *Acta Crystallogr. D 54*, 905−921.
45. Kurnikov, I. V. (2000) HARLEM molecular modeling package, v 1.0, Department of Chemistry, University of Pittsburgh, Pittsburgh, PA.
46. Nicholls, A., Sharp, K. A., and Honig, B. (1991) Protein folding and association: insights from the interfacial and thermodynamic properties of hydrocarbons, *Proteins 11*, 281−296.
47. Kraulis, J. P. (1991) MOLSCRIPT: a program to produce both detailed and schematic plots of protein structures, *J. Appl. Crystallogr. 24*, 946−950.
48. Merritt, E. A., and Bacon, D. J. (1997) RASTER3D: photorealistic molecular graphics, *Methods Enzymol. 277*, 505−524.
49. DeLano, W. L. (2002) The PyMOL molecular graphics system, Delano Scientific, San Carlos, CA.
50. Warshel, A., Chu, Z. T., and Parson, W. W. (1989) Dispersed polaron simulations of electron transfer in photosynthetic reaction centers, *Science 246*, 112−116.
51. Brooks, H. B., and Davidson, V. L. (1994) Kinetic and thermodynamic analysis of a physiologic intermolecular electron-transfer reaction between methylamine dehydrogenase and amicyanin, *Biochemistry 33*, 5696−5701.
52. Ivkovic-Jensen, M. M., and Kostic, N. M. (1997) Effects of viscosity and temperature on the kinetics of the electron-transfer reaction between the triplet state of zinc cytochrome c and cupriplastocyanin, *Biochemistry 36*, 8135−8144.
53. Lanzilotta, W. N., Parker, V. D., and Seefeldt, L. C. (1998) Electron transfer in nitrogenase analyzed by Marcus theory: evidence for gating by MgATP, *Biochemistry 37*, 399−407.
54. Davies, M. D., Qin, L., Beck, J. L., Suslick, K. S., Koga, H., Horiuchi, T., and Sligar, S. G. (1990) Putidaredoxin reduction of cytochrome P450cam—Dependence of electron transfer on the identity of putidaredoxin's C-terminal amino acid, *J. Am. Chem. Soc. 112*, 7396−7398.
55. Davies, M. D., and Sligar, S. G. (1992) Genetic variants in the putidaredoxin-cytochrome P450cam electron-transfer complex: identification of the residue responsible for redox-state-dependent conformers, *Biochemistry 31*, 11383−11389.
56. Holden, M., Mayhew, M., Bunk, D., Roitberg, A., and Vilker, V. (1997) Probing the interactions of putidaredoxin with redox partners in camphor P450 5-monooxygenase by mutagenesis of surface residues, *J. Biol. Chem. 272*, 21720−21725.
57. Pederson, T. T., Austin, R. H., and Gunsalus, I. C. (1977) in *Microsomes and Drug Oxidations* (Ulrich, V., Ed.) pp 275−283, Pergamon Press, Elmsford, NY.
58. Peterson, J. A., and Mock, D. M. (1975) in *Cytochromes P450 and b_5* (Cooper, D. Y., Snyder, O. R., and Witmer, C., Eds.) pp 311−324, Plemun Press, New York.
59. Brewer, C. B., and Peterson, J. A. (1986) Single turnover studies with oxy-cytochrome P450cam, *Arch. Biochem. Biophys. 249*, 515−521.
60. Nagano, S., Shimada, H., Tarumi, A., Hishiki, T., Kimata-Ariga, Y., Egawa, T., Suematsu, M., Park, S. Y., Adachi, S., Shiro, Y., and Ishimura, Y. (2003) Infrared spectroscopic and mutational studies on putidaredoxin-induced conformational changes in ferrous CO-P450cam, *Biochemistry 42*, 14507−14514.
61. Peterson, J. A., and Mock, D. M. (1979) Cytochrome P450cam and putidaredoxin interaction during electron transfer, *Acta Biol. Med. Germ. 38*, 153−162.
62. Furukawa, Y., and Morishima, I. (2001) The role of water molecules in the association of cytochrome P450cam with putidaredoxin, *J. Biol. Chem. 276*, 12983−12990.
63. Sevrioukova, I. F., Hazzard, J. T., Tollin, G., and Poulos, T. L. (2001) Laser flash induced electron transfer in P450cam monooxygenase: Putidaredoxin reductase−putidaredoxin interaction, *Biochemistry 40*, 10592−10600.
64. Aoki, M., Ishimori, K., and Morishima, I. (1998) Roles of negatively charged surface residues of putidaredoxin in interactions

with redox partners in P450cam monooxygenase system, *Biochim. Biophys. Acta 1386*, 157−167.
65. Hintz, M. J., and Peterson, J. A. (1981) The kinetics of reduction of cytochrome P450cam by reduced putidaredoxin, *J. Biol. Chem. 256*, 6721−6728.
66. Nakamura, K., Horiuchi, T., Yasukochi, T., Sekimizu, K., Hara, T., and Sagara, Y. (1994) Significant contribution of arginine 112 and its positive charge of *Pseudomonas putida* cytochrome P450cam in the electron transport from putidaredoxin, *Biochim. Biophys. Acta 1207*, 40−48.
67. Stayton, P. S., and Sligar, S. G. (1991) Structural microheterogeneity of a tryptophan residue required for efficient biological electron transfer between putidaredoxin and cytochrome P450cam, *Biochemistry 30*, 1845−1851.
68. Shimada, H., Nagano, S., Ariga, Y., Unno, M., Egawa, T., Hishiki, T., Ishimura, Y., Masuya, F., Obata, T., and Hori, H. (1999) Putidaredoxin-cytochrome P450cam interaction. Spin state of the heme iron modulates putidaredoxin structure, *J. Biol. Chem. 274*, 9363−9369.
69. Lo, K. K., Wong, L. L., and Hill, H. A. (1999) Surface-modified mutants of cytochrome P450cam: enzymatic properties and electrochemistry, *FEBS Lett. 451*, 342−346.
70. Roitberg, A. E., Holden, M. J., Mayhew, M. P., Kurnikov, I. V., Beratan, D. N., and Vilker, V. L. (1998) Binding and electron transfer between putidaredoxin and cytochrome P450cam−Theory and experiments, *J. Am. Chem. Soc. 120*, 8927−8932.
71. Sligar, S. G., and Gunsalus, I. C. (1976) A thermodynamic model of regulation: modulation of redox equilibria in camphor monooxygenase, *Proc. Natl. Acad. Sci. U.S.A. 73*, 1078−1082.
72. Hintz, M. J., Mock, D. M., Peterson, L. L., Tuttle, K., and Peterson, J. A. (1982) Equilibrium and kinetic studies of the interaction of cytochrome P450cam and putidaredoxin, *J. Biol. Chem. 257*, 14324−14332.
73. Page, C. C., Moser, C. C., Chen, X., and Dutton, P. L. (1999) Natural engineering principles of electron tunnelling in biological oxidation-reduction, *Nature 402*, 47−52.
74. Dus, K., Lipscomb, J. D., and Gunsalus, I. C. (1971) Abstracts of the 162nd American Chemical Society Meeting, Washington, D.C., Sept 12−17, 1971.
75. Shiro, Y., Iizuka, T., Makino, R., Ishimura, Y., and Morishima, I. (1989) ^{15}N NMR study on cyanide (C^{15}N-) complex of cytochrome P450cam. Effects of d-camphor and putidaredoxin on the iron-ligand structure, *J. Am. Chem. Soc. 111*, 7707−7711.
76. Sjodin, T., Christian, J. F., Macdonald, I. D., Davydov, R., Unno, M., Sligar, S. G., Hoffman, B. M., and Champion, P. M. (2001) Resonance Raman and EPR investigations of the D251N oxycytochrome P450cam/putidaredoxin complex, *Biochemistry 40*, 6852−6859.
77. Stayton, P. S., Poulos, T. L., and Sligar, S. G. (1989) Putidaredoxin competitively inhibits cytochrome b_5-cytochrome P450cam association: a proposed molecular model for a cytochrome P-450cam electron-transfer complex, *Biochemistry 28*, 8201−8205.
78. CCP4 (1994) Collaborative Computational Project Number 4. The CCP4 suite programs for protein crystallography, *Acta Crystallogr. D 50*, 760−763.
79. Poulos, T. L., Finzel, B. C., Gunsalus, I. C., Wagner, G. C., and Kraut, J. (1985) The 2.6 Å crystal structure of *Pseudomonas putida* cytochrome P450, *J. Biol. Chem. 260*, 16122−30.

BI0611154